PERGAMON

Vision Research 42 (2002) 1017–1033

Vision Research

www.elsevier.com/locate/visres

On the classification of simple and complex cells

Ferenc Mechler [a], Dario L. Ringach [b,*]

[a] Department of Neurology and Neuroscience, Weill Medical College of Cornell University, New York, NY 10021, USA
[b] Department of Neurobiology and Psychology, Brain Research Institute, Room 8441B, Franz Hall, University of California, Los Angeles, CA 90095-1563, USA

Received 19 September 2001; received in revised form 9 January 2002

Abstract

In their pioneering studies of primary visual cortex, Hubel and Wiesel described the existence of two classes of cells, which they termed "simple" and "complex". The original classification scheme was based on a number of partly subjective tests of linear spatial summation. Later, investigators adopted an objective classification method based on the ratio between the amplitude of the first harmonic of the response and the mean spike rate (or the F_1/F_0 ratio) when the neuron is stimulated with drifting sinusoidal gratings. This measure is bimodally distributed over the population and divides neurons into two classes that correspond closely to the classical definition by Hubel and Wiesel. Here we show that a simple rectification model can predict the observed bimodal distribution of F_1/F_0 in primary visual cortex when the distributions of the intracellular response modulation and mean are unimodal. Thus, contrary to common belief, the bimodality of F_1/F_0 does not necessarily imply the existence of two discrete cell classes. Furthermore, in reviewing the literature, we find no independent support for a simple/complex dichotomy. These results suggest that the existence of two distinct neural populations in primary visual cortex, and the associated hierarchical model of receptive field organization, need to be re-evaluated.

Keywords: Classification; Bimodal distribution; Clustering; Sigmoid non-linearity; V1 neurons

1. Introduction

In their early work on primary visual cortex, Hubel and Wiesel described the existence of two classes of cells: simple and complex (Hubel & Wiesel, 1962, 1968). A simple cell was defined as one that (a) had spatially segregated ON and OFF subregions, (b) exhibited summation within each region, (c) had ON and OFF subregions that were antagonistic and (d) it was possible to predict the neuron's response to any stimulus from the arrangement of excitatory and inhibitory subregions. If a neuron failed to pass one of these criteria it was defined as complex. Because some of these tests were qualitative in nature, difficult to apply consistently across laboratories, and based on manual plotting of the receptive field, researchers sought to replace them with quantitative measures that could be used to differentiate between simple and complex cells. With the advent of linear system theory in visual neuroscience it was realized that a key property being tested by Hubel and Wiesel's criteria was the linearity of spatial summation within the receptive field (De Valois, Albrecht, & Thorell, 1982; Maffei & Fiorentini, 1973; Movshon, Thompson, & Tolhurst, 1978b; Skottun et al., 1991). A number of investigators converged to propose that an appropriate measure of response linearity is the ratio between the amplitude of the first harmonic of the response and the mean spike rate (or the F_1/F_0 ratio) when the neuron is stimulated with drifting sinusoidal gratings (Skottun et al., 1991). These authors showed that the F_1/F_0 ratio is bimodally distributed over the V1 population. Furthermore, they established that the resulting classification corresponded closely to the classical definition of simple and complex cells by Hubel and Wiesel. The bimodal distribution of the F_1/F_0 ratio was taken as compelling evidence for the existence of discrete classes of simple and complex cells in V1. Due to its simplicity and ease of measurement, the F_1/F_0 ratio has become the standard used by visual neuroscientist to classify simple and complex cells.

Here we show that a simple rectification model can predict the observed bimodal distribution of F_1/F_0 in

* Corresponding author. Tel.: +1-310-206-5461; fax: +1-310-206-5895.
E-mail address: dario@ucla.edu (D.L. Ringach).

0042-6989/02/$ - see front matter
PII: S0042-6989(02)00025-1

primary visual cortex when the distributions of the intracellular response modulation and mean are unimodal. The basic result of our study can be explained intuitively with an analogy (Fig. 1). Assume we measure the height of the world population and observe that the resulting distribution is bimodal (Fig. 1(a)). One would conclude that the data indicate the existence of two subpopulations of individuals (short and tall). It is later discovered, however, that the ruler used to measure the heights was non-linear. Fig. 1(b) shows the relationship between the true and the measured heights of this non-linear ruler. Such a ruler will cause the shape of the measured and true distributions to differ. In our example, the true distribution is in fact unimodal (Fig. 1(c)), but after being passed through the non-linear ruler (Fig. 1(b)) it results in the observed bimodal distribution (Fig. 1(a)). The discovery of a non-linear ruler should prompt a revision of the initial inference about the presence of two discrete sub-populations. Our main finding can be stated as follows: neural rectification due to spike generation, together with the F_1/F_0 statistic, behaves as a non-linear ruler with respect to the relevant intracellular variable.

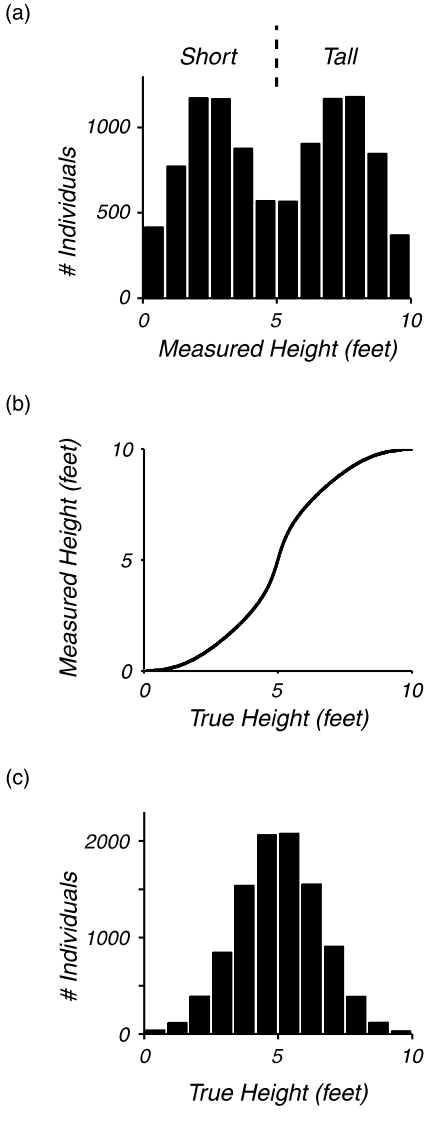

Fig. 1. The "non-linear ruler" analogy. (a) A bimodal distribution of measured heights over a population, (b) the non-linear ruler used in the measurement. The x-axis represents the true physical height and the y-axis the measured height, (c) the true underlying distribution of heights that, after being measured with the non-linear ruler, generates the bimodal distribution in (a).

A main conclusion from our study is that the bimodality of F_1/F_0 does not necessarily imply the existence of two discrete cell classes. In addition, in a comprehensive survey of the literature, we found no independent data to convincingly support the existence of discrete simple and complex cells classes. Taken together, these findings weaken the view of the cortex as being hierarchically organized into discrete classes of neurons. Instead, the converging evidence supports the existence of a continuum of cell properties and a uniform organization principle of cortical circuits.

2. Results

2.1. The rectification model

We assume that the time-modulation of the membrane voltage in cortical neurons in response to a drifting sinusoidal grating consists of a sinusoidal waveform of amplitude A, and mean V_{mean}, driven at the temporal frequency of the stimulus (Fig. 2). In addition, the instantaneous rate of firing of a neuron, $r(t)$, is assumed to be proportional to the supra-threshold membrane potential and zero if the membrane potential is below threshold,

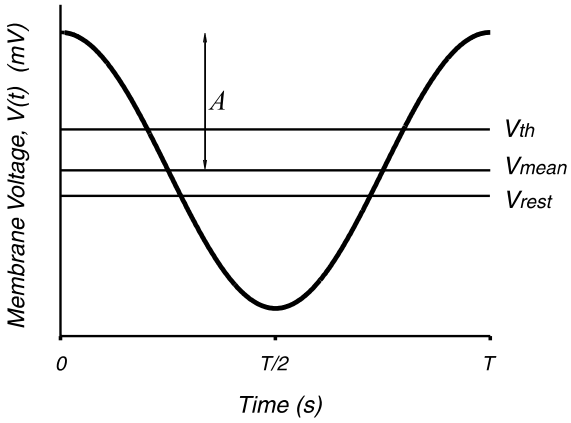

Fig. 2. The rectification model. The time-modulation of the membrane potential in response to a drifting sinusoidal grating is assumed to be a sinusoidal waveform with amplitude A, mean V_{mean} and period equal to that of the stimulus, T. V_{rest} represents the resting potential and V_{th} the threshold potential for spike generation.

$$r(t) = G[V_{\text{mean}} + A\cos(2\pi ft) - V_{\text{th}}]^{+}. \quad (1)$$

Here, f indicates the temporal frequency of the stimulus, $[x]^{+}$ represents half-rectification ($[x]^{+} = x$ if $x > 0$ and zero otherwise), V_{th} is the threshold for spike generation, and G represents the gain of the spike generator. The resting membrane potential of the neuron, when there is no visual stimulation, is denoted by V_{rest}. An ideal simple cell is expected to respond to a drifting sinusoidal grating with a large modulation amplitude, A, but with no significant changes in the mean ($V_{\text{mean}} \approx V_{\text{rest}}$). An ideal complex cell will respond with a significant increase in the mean ($V_{\text{mean}} \gg V_{\text{rest}}$), but little or no modulation, $A \approx 0$. Admittedly, this is a simplified model that does not capture the details of the biophysics but, nevertheless, summarizes nicely the relationship between the intracellular voltage and extracellular firing rates in cat area 17 (Carandini & Ferster, 2000).

The F_1/F_0 ratio of the response is a statistic on the spike rate modulation, $r(t)$, as measured with extracellular recordings. To see how this statistic depends on the intracellular variables we can rewrite Eq. (1) as:

$$\begin{aligned} r(t) &= G[V_{\text{mean}} + A\cos(2\pi ft) - V_{\text{th}}]^{+} \\ &= [a\cos(2\pi ft) - b]^{+}. \end{aligned} \quad (2)$$

Here, we used $G[x]^{+} = [Gx]^{+}$ for $G \geqslant 0$, and defined $a \equiv GA$ and $b \equiv G(V_{\text{th}} - V_{\text{mean}})$. If we denote $\chi = b/a$, the F_1/F_0 ratio can be written as (see Appendix A):

$$F_1/F_0 = \frac{-\chi\sqrt{1-\chi^2} + \arccos(\chi)}{\sqrt{1-\chi^2} - \chi\arccos(\chi)} \quad \text{if } -1 \leqslant \chi \leqslant 1, \quad (3a)$$

$$F_1/F_0 = -1/\chi \quad \text{if } \chi < -1, \quad (3b)$$

and F_1/F_0 is undefined for $\chi > 1$, as in this case the response is zero. The F_1/F_0 ratio depends only on the ratio between b and a, and not their absolute magnitudes. We denote by $F_1/F_0 = g(\chi)$ the function mapping χ into F_1/F_0. Fig. 3(a) depicts a plot of this function, and Fig. 3(b) shows its derivative, which measures the rate of change of $g(\chi)$. The function $g(\chi)$ is clearly non-linear; it has a sigmoid shape. For $\chi < -2$ we see that $F_1/F_0 < 0.5$ and the function changes at a slow rate. For increasing values of χ, the function $g(\chi)$ accelerates rapidly and crosses the $(\chi, F_1/F_0) = (-1, 1)$ point with maximum slope (Fig. 3(b)). For $\chi > -1$ the curve decelerates. We observe that $g(\chi)$ is convex in $(-\infty, -1)$ and concave in $(-1, 1)$.

As a consequence of this non-linearity, a unimodal distribution of a, b, and χ, can yield a bimodal distribution of the F_1/F_0 ratio (note that if one assumes a constant V_{th} and G, the *shape* of the distributions for a and b are the same as those of the response amplitude, A, and mean, V_{mean}, respectively). As an example, assume that a is distributed as $p(a) = 2/\sqrt{2\pi\sigma_a^2}\exp\left(-a^2/2\sigma_a^2\right)$ for $a \geqslant 0$ and zero otherwise (a half Gaussian distribution), and that b is independent of a, and Gaussian distributed, $p(b) = 1/\sqrt{2\pi\sigma_b^2}\exp(-b^2/2\sigma_b^2)$. Their ratio, $\chi = b/a$, will be Cauchy distributed, $p(\chi) = \pi^{-1}\alpha/(\alpha^2 + \chi^2)$, with $\alpha = \sigma_b/\ \sigma_a$. If we assume χ to have the particular Cauchy density shown in Fig. 4(a), the resulting distribution of the F_1/F_0 ratio is bimodal (Hartigan's dip statistic (Hartigan & Hartigan, 1985), $p < 10^{-5}$, significance obtained via Monte Carlo simulation with $N = 10^5$) with a dip at $F_1/F_0 = 1$ and modes at around $F_1/F_0 = 0$ and $F_1/F_0 = \pi/2 \approx 1.57$ (Fig. 4(b)). The reason for this behavior is that the probability density function of F_1/F_0 and χ are related by $p(F_1/F_0) = p(\chi)/|g'(\chi)|$ (Papoulis, 1984). This means that, in general, there will be a tendency for a low density in the distribution of F_1/F_0 in those locations where $g'(\chi)$ is large. In this case this happens at $\chi = -1$ which corresponds to $F_1/F_0 = 1$.

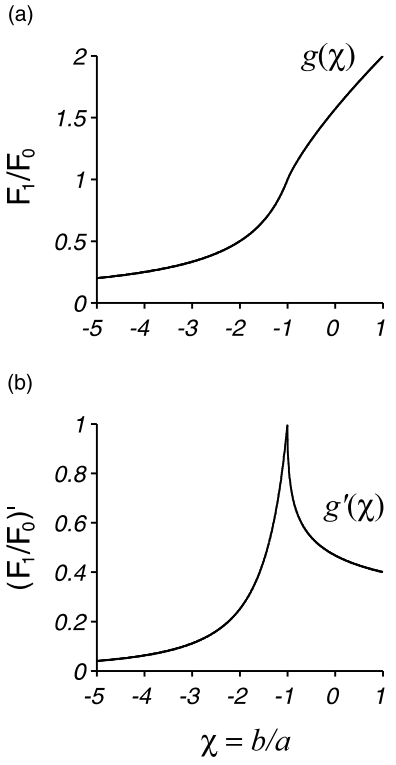

Fig. 3. Non-linear mapping between χ and the F_1/F_0 ratio. (a) The function $g(\chi)$ mapping χ into F_1/F_0, (b) plot of the derivative $g'(\chi)$.

The result can also be understood intuitively. The mode near 1.57 is due to the concentration of a significant mass of χ near zero. A value of $\chi = 0$ (when the mean membrane potential equals the threshold for rectification) maps to the F_1/F_0 ratio expected for half-rectification of a sinusoid (or $\pi/2 \approx 1.57$). Similarly, the mode of F_1/F_0 near zero is formed by the mass of χ present in the long left tail of the Cauchy density that, for values of $\chi < -2$, maps to values of F_1/F_0 less than 0.5. The right tail of χ is not relevant, as values of $\chi > 1$

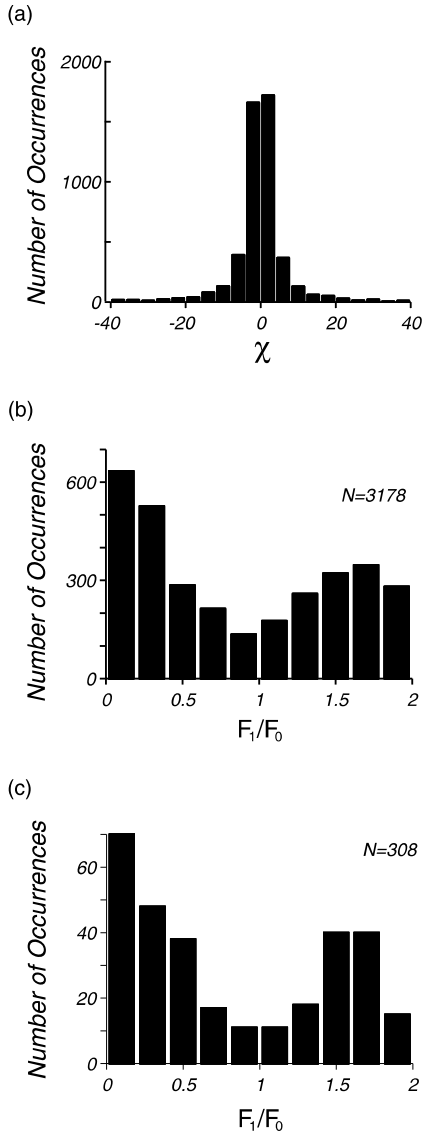

Fig. 4. The rectification model generates a bimodal distribution of F_1/F_0 indistinguishable from experimental data. (a) Distribution of χ assuming normal distributions of a and b for a choice of the scale parameter $\alpha = \sigma_b/\sigma_a = 2.2$, (b) the resulting distribution of F_1/F_0 obtained from sampling $N = 5000$ points in the rectification model (points with $\chi \geqslant 1$ were discarded, resulting in a total effective count of $N = 3178$), (c) distribution of F_1/F_0 in monkey primary visual cortex (Ringach et al., unpublished data). These data were obtained with drifting luminance gratings of optimal spatiotemporal parameters. The contrast was high (80–99%).

generate a zero response and the F_1/F_0 ratio is therefore undefined. Finally, the dip at $F_1/F_0 = 1$ is due to the relatively large slope of $g(\chi)$ which is maximal at $(\chi, F_1/F_0) = (-1, 1)$ (Fig. 3). This large slope means that the range of χ values that map to values of F_1/F_0 close to one is relatively small. Thus, the probability of observing $F_1/F_0 \approx 1$ is relatively low and one observes a dip of the distribution at this location. The rectification model does not only predict a bimodal distribution of F_1/F_0 but also the location of the dip at one.

There is nothing peculiar about this example. Other probability density functions with similar characteristics would also generate a bimodal distribution of the F_1/F_0 ratio. We demonstrate below that similar results are also obtained if the intracellular response is not a sinusoidal waveform, or if the threshold non-linearity is not a perfect rectifier. Other choices for these functions will also yield a sigmoidal mapping function $g(\chi)$, which by virtue of the relationship $p(F_1/F_0) = p(\chi)/|g'(\chi)|$ can generate bimodal distributions of the F_1/F_0 ratio for some unimodal distributions of χ. This formula also makes evident the fact that the shape of $p(\chi)$, determined by the distribution of a and b, also influences the shape of $p(F_1/F_0)$.

To compare the predictions of the model with experimental data, the measured distribution of F_1/F_0 in macaque primary visual cortex is shown in Fig. 4(c). The empirical F_1/F_0 distribution is bimodal (dip statistic, $p < 10^{-5}$). Furthermore, the model and empirical distributions are statistically indistinguishable (single sample Kolmogorov–Smirnov test, $p > 0.14$). Thus, one cannot reject the hypothesis that the data came from the rectification model. This is remarkable, as it shows that a one-parameter model can explain the distribution of F_1/F_0 in primary visual cortex (the only parameter is the scale of the Cauchy distribution, α). We conclude that the bimodality of F_1/F_0 could originate, in principle, from a simple non-linear system where both the intracellular response modulation and mean are unimodal.

We note that in the original definition of the F_1/F_0 ratio the neuron's spontaneous rate is subtracted from the stimulus evoked mean spike rate to calculate the effective F_0 component (De Valois et al., 1982; Skottun et al., 1991). The rectification model does not incorporate this fact. Effectively we are assuming a spontaneous rate of zero. This simplifies the mathematical analysis and is reasonable given that the large majority of cortical cells have very low spontaneous rates. Nevertheless, we verified via computer simulations that subtracting the spontaneous spike rate, when the distribution of spontaneous activity matches the one observed in the cortex, has little effect on our results (data not shown).

2.2. Robustness of the rectification model

Even though the half-rectifier model provides accurate descriptions of the firing rates of real neurons, both in vitro (Carandini, Mechler, Leonard, & Movshon, 1996) and in vivo (Carandini & Ferster, 2000), it may still be perceived as a rather simplified model of the biophysics of spike generation. This may raise questions as to the robustness of our findings. First, one may ask how robust the bimodality of F_1/F_0 is to changes in the shape of the spike-generator non-linearity, or when the shape of the underlying modulation departs from a perfect sinusoidal function. Second, one may ask what

would be the prediction if we were to consider a more "realistic" biophysical model of a neuron.

To study how the shape of the output non-linearity influences the results, we computed the predicted F_1/F_0 distributions for power functions with different exponents (Fig. 5, across columns). These power functions were chosen to span a range of spike generator non-linearities: (a) a square-root non-linearity, (b) a linear or half-wave rectifier, and (c) a half-squaring operator. To compare them on an equal footing, the three non-linearities (top row) are fed the same set of inputs (sinusoidal modulations). Therefore, the associated intracellular ratio parameter, χ, is identically distributed in all conditions (second row). The values of χ are passed through the corresponding non-linear transducer function $g(\chi) : \chi \rightarrow F_1/F_0$ (third row), which transforms the unimodal distribution of χ into the resulting F_1/F_0 distributions (bottom row). Bimodality is evident in all these distributions, with the dip always near one. However, both the depth and exact location of the dip in the F_1/F_0 distribution (indicated by the arrows) systematically depend on the power of the non-linearity. An increasing exponent of the power function results in a decreasing peak slope of $g(\chi)$ (vertical arrows in forth row) and an increase in the value of $g(\chi)$ at all points. This causes the same χ values to be mapped to higher values of F_1/F_0, thereby increasing the relative proportion of "simple" cells in the distribution. In general, V1 neurons exhibit a distribution of exponents (Albrecht & Geisler, 1991; Anzai, Ohzawa, & Freeman, 1999) and

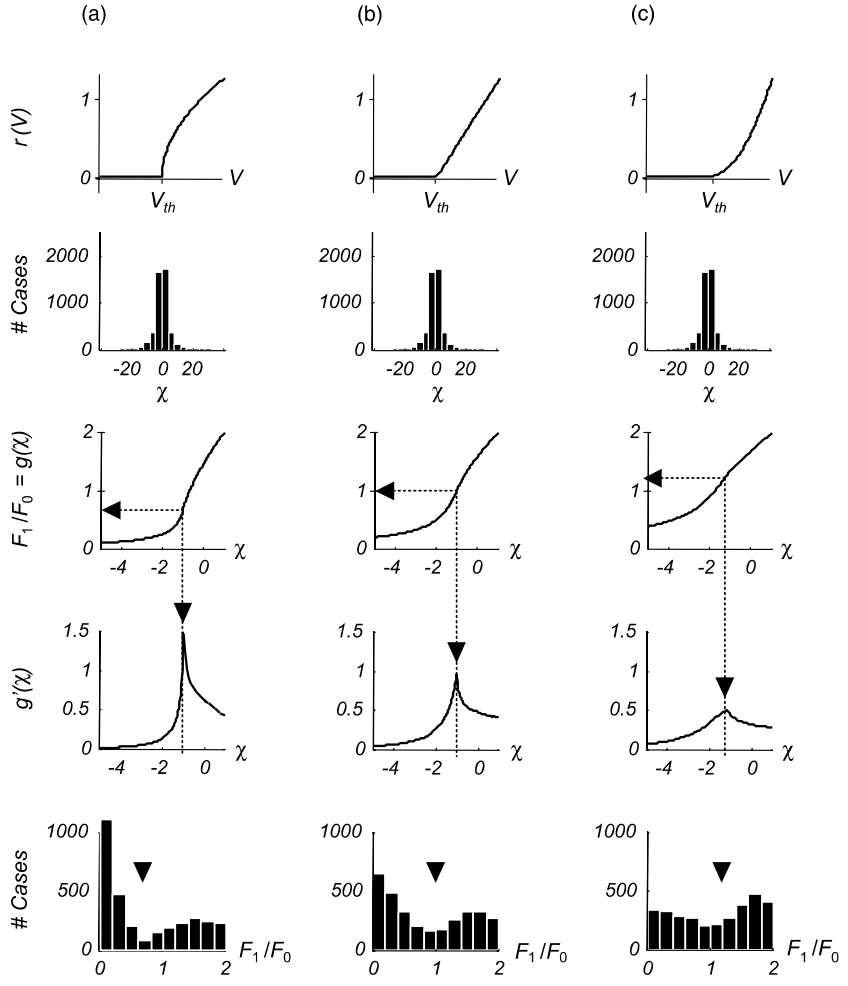

Fig. 5. Dependence of the F_1/F_0 distribution on the shape of the output non-linearity. Given the intracellular potential, V, the modeled operators generate spike rate responses $r(V)$ that are power functions, with different exponents p, of the supra-threshold intracellular potential $r(V) = 0$, $V < V_{\text{th}}$, $r(V) = (V - V_{\text{th}})^p$, $V \geqslant V_{\text{th}}$. The three selected non-linearities, shown in the first row are (a) square root operator, $p = 0.5$ (b) half-wave rectifier, $p = 1.0$ and (c) half-squaring operator, $p = 2.0$. Second row: each spike rate operator receives for input a large set of sinusoidal modulations of the intracellular potential $V(t) = a\cos(t) - b$ where a and b are independently distributed and normal (or half-normal) and whose associated ratio parameter $\chi = b/a$ is identically distributed for all conditions, and Cauchy distributed with $\alpha = 2.2$, $N = 5000$ as before. Third row: $g(p, \chi) = \chi \rightarrow F_1/F_0$, the transducer function associated with the power-low operator of exponent p (see Appendix A). Fourth row: $g'(p, \chi)$ the derivative of the transducer function. Arrows indicate maximum slope and value of $g(p, \chi)$. Bottom row: the resulting distribution of the F_1/F_0 ratio ($N = 3176$).

the expected distribution can be thought of as a mixture of the predicted F_1/F_0 distributions.

Next, we examine how the shape of the membrane voltage modulation influences the F_1/F_0 distribution by comparing samples from a continuum of distorted cosines (Fig. 6). The three functions chosen, shown on the top row of Fig. 6, represent samples of von Mises functions and their inverted versions. They are selected to mimic some of the distortions observed in the postsynaptic membrane potentials (see e.g., Jagadeesh, Wheat, Kontsevich, Tyler, & Ferster, 1997, Lampl, Anderson, Gillespie, & Ferster, 2001). The function in the middle (Fig. 6(b)) is an undistorted cosine. The voltage modulation on the left (Fig. 6(a)) is a periodic function with a broad peak and a narrow trough, while the function on the right (Fig. 6(c)) has a broad trough and a narrow peak. Each function has zero mean, and is normalized to have a minimum value of -1. The normalization at the minimum is required to guarantee a common scale of comparison for the intracellular ratio parameter, χ. To put the comparison on equal footing, the same threshold non-linearity (half-wave rectification) and identically distributed χ (second row) are used. As before, we observe that all resulting F_1/F_0 distributions are bimodal with dips near one. However, the exact location of the dip and the degree of bimodality varies. The maximum slope of $g(\chi)$ increases as the peak of the modulation becomes sharper and the trough broader (Fig. 6, fourth row). This contributes to enhance the bimodality in the F_1/F_0 distribution. We also see an increase in $g(\chi)$ as the peak of the modulation becomes narrower. Again, this causes the same χ values to be mapped to higher values of F_1/F_0 thereby increasing the relative proportion of "simple" cells. In general one observes a distribution of shapes for the intracellular modulation (Jagadeesh et al., 1997, Lampl

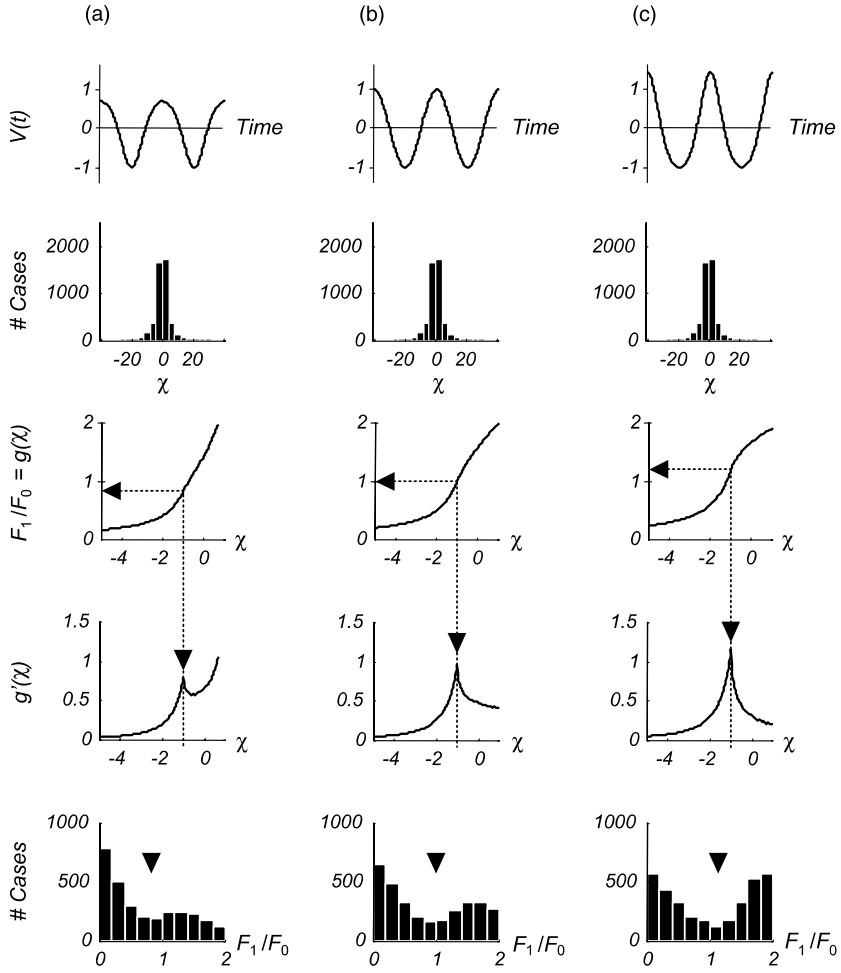

Fig. 6. Dependence of the F_1/F_0 distribution on the shape of the intracellular voltage modulation. Top row: three possible shapes of $V(t)$ obtained as versions of the von Mises function, $M(t) = C_1(C_0 + \mathrm{sign}(\kappa)\exp^{|\kappa|\cos(t)})$ with parameter κ. The value of C_0 was first chosen so that the mean of the waveform was zero. The value of C_1 was then chosen so that $\min_t(M) = -1$. Voltage modulations are considered to be of the form $V(t) = aM(t) - b$, where a is the modulation amplitude; b is the mean potential deviation from threshold, where a and b are distributed as before. (a) $\kappa = -0.75$, produces a broad peak with a narrow trough, (b) $\kappa = 0$, an undistorted cosine, (c) $\kappa = +0.75$, mirror-symmetric image of (a) around the y-axis. The rest of the figure follows the same organization as Fig. 5.

et al., 2001) and the empirical distribution can be expected to be a mixture of the predicted F_1/F_0 distributions.

In the rectification model we assumed that the variables a and b are independent. However, it is possible that real data will show a correlation between the DC and amplitude modulation evoked by visual stimulation. If a and b are jointly normal with a correlation coefficient of $r \neq 0$, the resulting distribution of χ will not be centered at zero but at $r\sigma_b/\sigma_a$. In Fig. 7(a–c) we explore how the shape of F_1/F_0 changes when the variables a and b are positively correlated (Fig. 7(a), $r = +0.45$), uncorrelated (Fig. 7(b), $r = 0$), or negatively correlated (Fig. 7(c), $r = -0.45$). For $\alpha = \sigma_b/\sigma_a = 2.2$ the selected correlation values induce a unit step shift in the distribution of χ in either the positive or negative directions. In these simulations, we assumed half-wave rectification and a perfect sinusoidal modulation. A bimodal distribution F_1/F_0 is observed in all three cases, with a dip near one in all conditions. The exact location of the dip and the degree of bimodality depend on the correlation. As a and b become positively correlated the bimodality is enhanced and the relative number of "simple" cells increases.

There are further departures from the assumptions of the basic rectification model one may want explore, such as changes in mean and shape of the distributions of a and b. For example, global changes in cortical excitability may be represented in the model as a change in the mean of b. Similarly, the fact that many cortical neurons receive a substantial (time-modulated) input from the lateral geniculate nucleus may imply a distribution of a that has a mode at a location above zero. We have explored changes in these variables in some detail and found, once again, that the degree of bimodality and the relative number of simple versus complex cells can be altered by a manipulation of these parameters (data not shown).

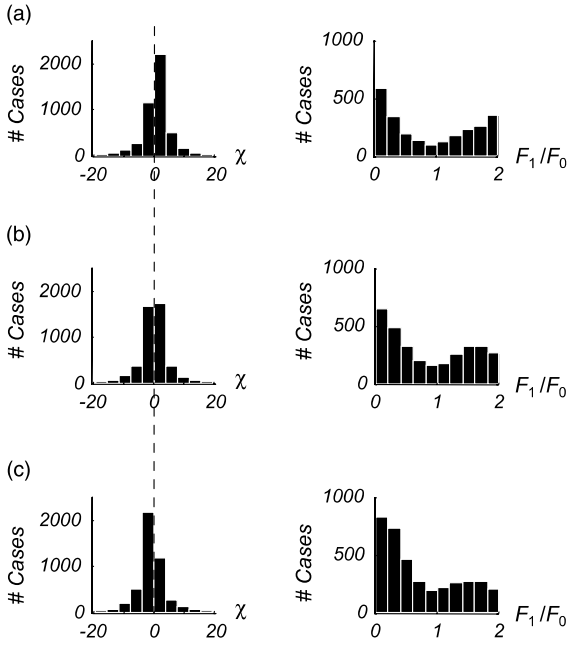

Fig. 7. Dependence of the F_1/F_0 distribution on the correlation between a and b. A correlation between a and b produces a shift in the distribution of χ. (a) Cauchy, with shape parameter $\alpha = 2.2$ and correlation $r = 0.45$ is centered at $\chi = +1$, (b) Cauchy, with shape parameter $\alpha = 2.2$ and correlation $r = 0$ is centered at $\chi = 0$, (c) Cauchy, with shape parameter $\alpha = 2.2$ and correlation $r = -0.45$ is centered at $\chi = -1$.

The simulations presented here are not exhaustive in the sense that many possible combinations of the various factors mentioned above have not been studied. It should be evident, however, that a complete study of all possible combinations is unfeasible given the number of parameters involved. Nevertheless, we feel the numerical studies presented here provide a full account of the types of departures in the F_1/F_0 distribution one could expect from that obtained with the basic rectification model. The bimodality of the F_1/F_0 ratio appears to be a rather robust phenomenon that is observed under a wide variety of conditions.

Finally, it has recently been shown that a realistic large-scale model of primary visual cortex, which takes into account V1 micro-anatomy and uses conductance-based integrate-and-fire neurons, can yield a bimodal distribution of the F_1/F_0 (Tao, Shelley, Shapley, & McLaughlin, 2001). In this detailed model, however, all the parameters governing the intrinsic dynamics of the neurons and the connectivity between them have unimodal distributions. Thus, detailed biophysical models can also exhibit the type of phenomenon discussed in this study. We think the simple rectification model provides a parsimonious explanation of these results and, despite its simplicity, captures the key mathematical aspects underlying the bimodality of the F_1/F_0 ratio in more detailed biophysical models.

2.3. Relationship between the intracellular and extracellular modulation ratios

Carandini and Ferster (2000) defined a quantity analogous to the F_1/F_0 spike modulation ratio based on the time-modulation of the intracellular membrane potential. We follow their work and define f_1/f_0 as the intracellular modulation ratio, where $f_1 = a$ and $f_0 = V_{\text{mean}} - V_{\text{rest}}$. A final question of interest we want to address here is the relationship between the extracellular F_1/F_0 and the intracellular f_1/f_0.

First, notice that $f_0 = (V_{\text{th}} - V_{\text{rest}}) - b$. Therefore f_1/f_0 is not simply proportional to $1/\chi = a/b = a/(V_{\text{th}} - V_{\text{mean}})$. Instead, f_1/f_0, unlike F_1/F_0, depends on both a and b, not just their ratio (see Appendix A). This means, that the $f_1/f_0 \rightarrow F_1/F_0$ mapping is not a one-to-one

function. To avoid potential confusion, it is useful to keep in mind that while the f_1/f_0 ratio might be an appropriate quantity to define "simple" and "complex" cells—with $f_1/f_0 > 1$ indicating the predominance of the linear response, and $|f_1/f_0| < 1$, the predominance of spatiotemporal non-linearities—it is the χ variable that is the mathematically relevant intracellular quantity for determining the extracellular F_1/F_0 modulation ratio.

To examine how f_1/f_0 relates to F_1/F_0 we construct a model along the same principles as above. As before, we assume a half-wave rectifier and sinusoidal inputs. The intracellular parameters are the modulation amplitude a (half-Gaussian, with standard deviation σ_a) and the voltage distance from threshold b (Gaussian, with standard deviation σ_b). These variables are assumed to be independently distributed, so their ratio, $\chi = b/a$, is Cauchy distributed with a scale parameter of $\alpha = \sigma_b/\sigma_a$. The parameter α measures the relative spread of the DC distribution with respect that of first-harmonic amplitude. We also define a second parameter, β, as $\beta = \sigma_a/(V_{\text{th}} - V_{\text{rest}})$. Notice that β measures the degree of intracellular amplitude modulation in units of the voltage "distance" from threshold. In this model, the parameters α and β can be varied independently.

The $f_1/f_0 \rightarrow F_1/F_0$ mapping is dependent on both α and β. Fig. 8 illustrates this dependence obtained by simulating $N = 10^6$ data points for each case. Each panel in the matrix of Fig. 8 shows results for a different combination of (α, β), whose corresponding values are indicated at the margins (sampled in logarithmic steps). The double-logarithmic scatter-plot shows the resulting distribution in the joint $(f_1/f_0, F_1/F_0)$ plane for the corresponding value of the parameters. The resulting gray-scale of a region in the scatter-plot is therefore proportional to the probability of occupancy in that region. Dark lines represent theoretical boundaries of the region that points can occupy in the $(f_1/f_0, F_1/F_0)$ plane (see Appendix A). Vertical dotted line depicts the conventional simple/complex boundary $F_1/F_0 = 1$. The horizontal dotted line corresponds to a constant intracellular modulation ratio $f_1/f_0 = 0.5$, suggested as boundary separating between simple and complex neurons (see Fig. 11 in Carandini & Ferster, 2000). In each case, the distribution of f_1/f_0, obtained as the marginal distribution of the scatter-plots along the y -axis, is included as an inset. As already shown, the distribution of χ and that of F_1/F_0 depend only on the value of α and do not change across the rows of the matrix. Thus, we plot these distributions as the bottom two rows in Fig. 8.

First, notice that for $\alpha = 1$, 1.5 and 2.2 the distributions of F_1/F_0 are bimodal with dips near one. However, all the corresponding intracellular distributions of f_1/f_0 are unimodal. Thus, a unimodal f_1/f_0 does not imply a unimodal F_1/F_0. We also observe that the relative numbers of "simple" versus "complex" cells in the F_1/F_0 distribution increases as α decreases.

Second, notice that the distribution of f_1/f_0 depends on β. As β increases the amount of mass probability around the mode at $f_1/f_0 = 0$ decreases and the tails become heavier. Therefore, if intracellular measurements are used to define a simple cell as one for which $f_1/f_0 > r_{\text{crit}}$, for a fixed criterion ratio r_{crit}, the relative number of simple versus complex cells will necessarily increase as β increases. On the other hand, the ratio between "simple" and "complex" based on F_1/F_0 will remain constant, as it depends solely on α. This provides another example demonstrating that a classification scheme based on the intracellular f_1/f_0 and the extracellular F_1/F_0 are not equivalent.

Third, if the shape of threshold non-linearity and the voltage modulation are known, the distribution of α and β can be estimated from the distribution of f_1/f_0 and F_1/F_0. To our knowledge, the only set of such data published is by Carandini and Ferster (2000) in cat area 17. To facilitate the comparison between the model's predictions with the neuronal data we generated the scatter-plots in Fig. 8 to resemble their Fig. 11. Unfortunately, because their data set is rather limited ($N = 28$) and biased (75% of their recordings were obtained from simple cells), it is not possible to perform such estimation nor to verify whether the intracellular f_1/f_0 distribution over the entire V1 population is unimodal or bimodal.

The rectification model can show a bimodal distribution for F_1/F_0 when f_1/f_0 has a unimodal distribution. However, the model does not rule out the possibility that f_1/f_0 is bimodal. Perhaps, sufficiently large and unbiased measurements of f_1/f_0 could demonstrate the existence of two discrete classes on neurons in V1.

3. Discussion

Our result could be considered an "existence proof" that a simple model, where all the physical parameters have unimodal distributions, can generate a bimodal distribution of the F_1/F_0 ratio that is indistinguishable from empirical data. The bimodality of the F_1/F_0 ratio, long considered as disproving the null hypothesis of a continuum of cell properties, should not be accepted as such. The findings do not prove conclusively that the "non-linear ruler effect" is indeed what is happening in V1. However, as we argue next, there appears to be no independent data to convincingly support the existence of discrete simple and complex cells classes. Thus, in our opinion, the question of whether there are simple and complex cell classes in V1 remains open.

Several measures have been proposed in the literature to distinguish between simple and complex cells. Because the concept of "spatial summation" was the basic idea behind Hubel and Wiesel's original classification scheme, the large majority of these investigations fo-

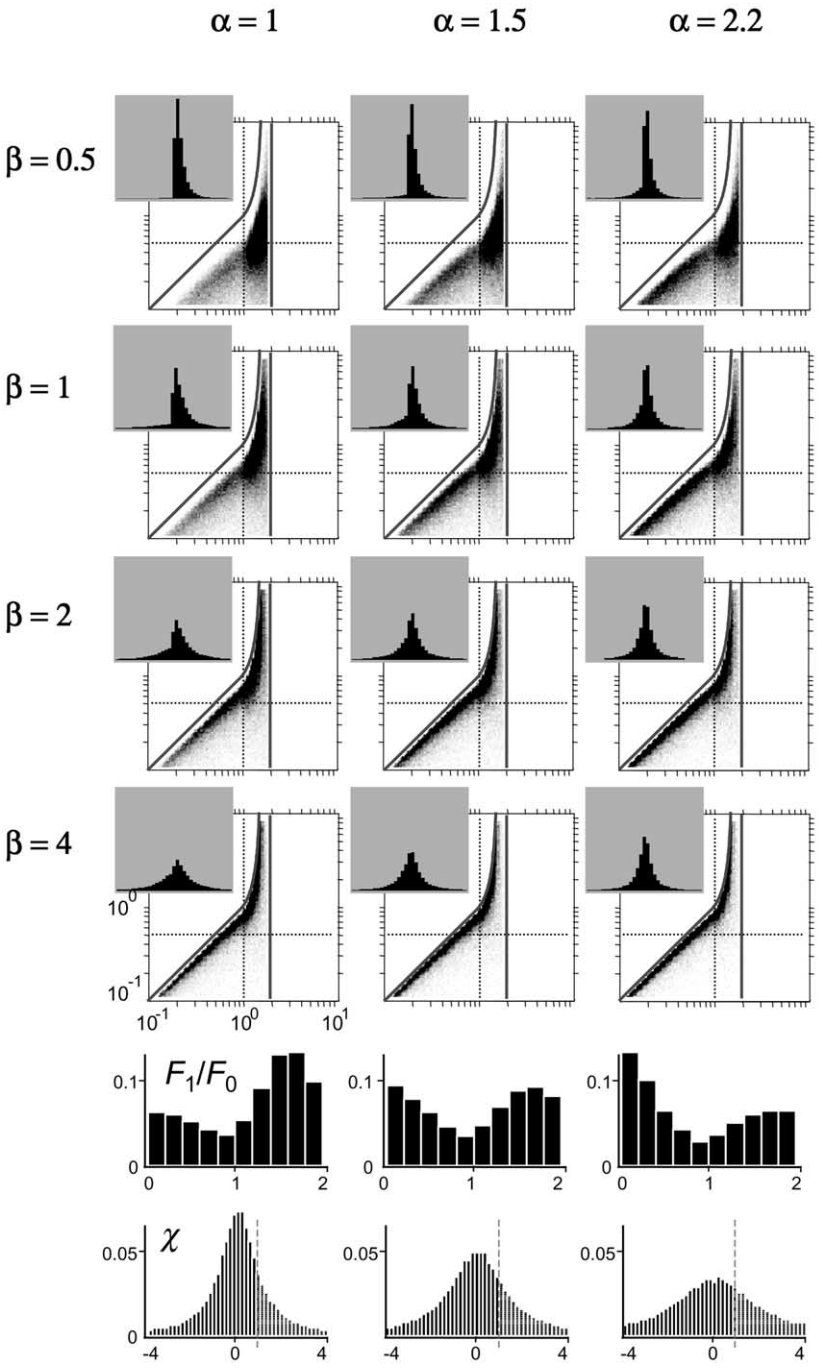

Fig. 8. Relationship between the f_1/f_0 intracellular (potential) modulation ratio and the F_1/F_0 extracellular (spike) modulation ratio predicted by the rectification model. Each panel in the matrix illustrates results for a different combination of (α, β) whose corresponding values are indicated at the margins. The double-logarithmic scatter-plot shows the resulting distribution in the joint $(f_1/f_0, F_1/F_0)$ plane for the corresponding value of the parameters. The distribution corresponds to a simulation of $N = 10^6$ points. For each (α, β) case, the distribution of f_1/f_0 obtained as the marginal distribution of the scatter-plots along the y-axis, is included as an inset. Note that this marginal distribution is on linear scale and includes cells whose mean potential response was hyperpolarizing and could not be shown in the scatter plot. The distribution of χ and that of F_1/F_0 (the marginal distribution along the x-axis) depend only on the value of α and do not change across the rows of the matrix. Thus, they are plotted separately as the two bottom rows of the Figure. The simple versus complex cell ratio obtained for the different values of α were (from left to right) 0.66, 0.53 and 0.42. See text for details.

cused on some aspect of spatial processing of the receptive field. Other measures, not directly linked to the spatial structure of the receptive field (such as spontaneous rate of activity, response variability, temporal tuning, color sensitivity, and ocular dominance) have been studied as well. If one of these measures showed a

bimodal distribution in V1 that corresponded closely to the classical definition by Hubel and Wiesel, and the measure were not subject to the phenomenon described here or other criticisms, one would have independent evidence for the existence of simple and complex classes of neurons. We reviewed the literature in search for such evidence.

Table 1 provides a summary of studies that have measured some property of visual responses in V1 and reported their results for the entire population. Some of these results are already reviewed in Dean and Tolhurst, 1983 and Skottun et al. (1991). The vast majority of studies do not show a bimodal distribution in V1 or the distributions were not reported and their shapes cannot be assessed. In cases where a dichotomy was reported, the measures used were often qualitative in nature. We focus the following discussion on studies that reported a bimodal distribution of a statistic and/or claimed separation between simple and complex cells.

A measure of receptive field linearity that has been argued to show a bimodal distribution in V1 is the ratio between the mean of the second harmonic amplitude to the maximum first harmonic amplitude (F_2/F_1) in contrast reversing sinusoidal gratings (Hawken & Parker, 1987). The mean and maximum are computed across a set of equally spaced spatial phases of a contrast reversing grating. Complex cells are expected to have $F_2/F_1 > 1$, while simple cells are expected to have $F_2/F_1 < 1$. We re-examined these data, which are replotted in Fig. 9(a) for convenience. The degree of bimodality in the F_2/F_1 ratio is much less pronounced than the one observed in the F_1/F_0 distribution, and a statistical test reveals that dip in the F_2/F_1 distribution is not statistically significant (dip-statistic, $p > 0.4$).

Another statistic, derived from the original Hubel and Wiesel's criteria, is the separation (or discreteness) of ON and OFF subfields. To the best of our knowledge, Schiller et al., 1976c is the only study reporting a significant bimodal distribution of subfield segregation (the data in their Fig. 20, statistic, $p < 10^{-2}$). These authors found that subfield separation is bimodally distributed with a dip at 0.1°. The method used to establish the separation between subfields involved drifting bright and dark edges across the receptive field at constant velocities. Time differences between the peaks in the PSTHs for bright and dark bars were converted into differences in space by multiplication with the stimulus velocity. This method is problematic because it confounds space and time: differences in the temporal response of ON and OFF subfields will be converted into differences in subfield segregation. As an example, a neuron with a single subfield but a biphasic temporal response may appear as having two segregated subregions. Another study (Dean & Tolhurst, 1983) estimated subfield segregation (or "discreteness") from line-weighting functions measured with bars of opposite contrast polarity and they reported a unimodal distribution in V1.

A number of studies have used the F_1/F_0 ratio (or a qualitative judgment of receptive field linearity) to first classify cells into simple and complex classes and then proceeded to test if these two groups differ statistically along other receptive field properties, such as their spontaneous spike rates (Gilbert, 1977), receptive field size (Hubel & Wiesel, 1962), ocular dominance (Schiller et al., 1976b) and color bandwidth (Thorell et al., 1984), among others. While such analyses may reveal statistical differences among simple and complex cells, the results should be interpreted with caution, as they could be a consequence of a correlation between a measure of receptive field linearity and the property under consideration. Specifically, these results could arise in systems where all the physical variables have (correlated) unimodal distributions. Such possibility is illustrated in Fig. 10. Assume the intracellular f_1/f_0 is correlated with P another measurable property of the receptive field (Fig. 10(a)). The distribution of f_1/f_0 in this example is unimodal (Fig. 10(b)). The distribution of P (not shown) is also unimodal and very similar to that of f_1/f_0 (Fig. 10(b)), which is a consequence of these two variables being correlated. However, when the F_1/F_0 ratio is calculated for this same population the distribution is bimodal (Fig. 10(c)). Importantly, the F_1/F_0 ratio and P are also correlated, as expected from the relationship between f_1/f_0 and F_1/F_0 (Fig. 8). This means that if simple and complex are now defined in terms of the F_1/F_0 ratio statistic (or an equivalent subjective classification), one finds that the mean value of the property P differs statistically between these two groups (Fig. 10(d)). This finding, however, should not be interpreted as meaning that "simple" and "complex" cells could be segregated using the property P. The distribution of P over the *entire* population should be evaluated first and, as we already pointed out, the distribution in this numerical simulation is unimodal and does not indicate the presence of two sub-populations. One of the several studies that have carried out such an analysis is considered next.

A neuron's spectral bandwidth has been argued to segregate simple and complex cells, with complex cells being more broadband tuned than simple cells (Thorell et al., 1984). These authors used the F_1/F_0 ratio to classify neurons and plotted separately the distribution of spectral bandwidth for simple and complex cells, which were statistically different. However, as described above, this result could be expected from a correlation between a unimodal f_1/f_0 and color bandwidth and does not necessarily imply that color bandwidth segregates simple and complex cells. Indeed, when the data in Fig. 5 in Thorell et al., 1984 are re-plotted across the entire V1 population the distribution of spectral bandwidths is unimodal (Fig. 9(b), dip-statistic, $p > 0.6$) and does not suggest the existence of two discrete classes of neurons.

Table 1
Some of the quantitative measures previously used to distinguish between "simple" and "complex"

Measure	Classification method[a]	Animal[b]	Distribution reported?	*N*	Claimed segregation?	Source
F_1/F_0	1	M	Yes	94	Yes	Schiller, Finlay, and Volman (1976a)
	3	C	Yes	1061	Yes	Skottun et al. (1991)
	3	C	Yes	391	No[c]	Dean and Tolhurst (1983)
	2	M	Yes	336	Yes	Cumming, Thomas, Parker, and Hawken (1999)
	3	M	Yes	343	Yes	De Valois et al. (1982)
Intracellular F_1/F_0	2	C	Yes	28	No	Carandini and Ferster (2000)
Spatial phase null test	**4**[d]	**M**	**Yes**	**138**	**Yes**	Hawken and Parker (1987**)**
ON/OFF segregation	1	C	No	303	Yes[e]	Hubel and Wiesel (1962)
	1	M	No	272	Yes[e]	Hubel and Wiesel (1968)
	1	**M**	**Yes**	**296**	**Yes**	**Schiller, Finlay, and Volman (1976c)**
	3	C	Yes	74	No	Dean and Tolhurst (1983)
Number of RF regions	3	C	Yes	110	No	Movshon, Thompson, and Tolhurst (1978a)
RF size	1	C	Yes	112	No	Hubel and Wiesel (1962)
	1	M	Yes	422	No	Schiller, Finlay, and Volman (1976c)
	1	C	Yes	56	No	Hammond and Munden (1990)
Length summation	1	M	Yes	355	No	Schiller et al. (1976c)
	1	C	Yes	87	No	Swindale and Cynader (1989)
End/side inhibition	2	C	Yes	82	No	De Angelis, Freeman, and Ohzawa (1994)
Area summation	2	M	Yes	85	No	Sceniak, Ringach, Hawken, and Shapley (1999)
Spatial frequency tuning	3	M	Yes	87	No	Schiller et al. (1976a)
	3	M	Yes	358	No	De Valois et al. (1982)
	4[d]	M	Yes	138	No	Hawken and Parker (1987)
	1	C	Yes	149	No	Movshon et al. (1978b)
Orientation selectivity	1	M	Yes	354	No	Schiller, Finlay, and Volman (1976b)
	1	C	Yes	77	No	Heggelund and Albus (1978)
Direction selectivity	4[d]	M	Yes	147	No	Hawken, Parker, and Lund (1988)
	3	C	Yes	176	No	Casanova, Nordmann, Ohzawa, and Freeman (1992)
Preferred phase/disparity	3	C	Yes	109	No	Ohzawa, De Angelis, and Freeman (1996, 1997)
Vernier offset	1	C	Yes	87	No	Swindale and Cynader (1989)
Spontaneous firing rates	4[f]	C	Yes	99	No	Pettigrew, Nikara, and Bishop (1968)
	NA	C	No	185	No	Tomko and Crapper (1974)
	1	M	Yes	382	No	Schiller et al. (1976c)
Response variability	1	M	Yes	333	No	Schiller, Finlay, and Volman (1976d)
	1	C	Yes	83	No	Heggelund and Albus (1978)
	NA	C	No	185	No	Tomko and Crapper (1974)
Bursting	1	C	No	57	Yes	Cattaneo, Maffei, and Morrone (1981)
	NA	C	Yes	507	No	De Busk, De Bruyn, Snider, Kabara, and Bonds (1997)
Contrast threshold and gain	3	C	Yes	43	No	Dean (1981)
Contrast sensitivity	1	C+M	No	114	No	Albrecht, Valois, and Thorell (1980)
Contrast threshold	2	C	Yes	48	No	Skottun, Bradley, Sclar, Ohzawa, and Freeman (1987)
Contrast gain control	3	C	Yes	36	No	Bonds (1991)
	3	C	Yes	83	No	Ohzawa, Sclar, and Freeman (1985)
Temporal frequency tuning	2	M	Yes	75	No	Hawken, Shapley, and Grosof (1996)
Response latency	NA	M	Yes	298	No	Maunsell and Gibson (1992)
Cone weights and ratios	2	M	Yes	104	No	Lennie, Krauskopf, and Sclar (1990)
Color/luminance sensitivity	1	M	Yes	171	No	Thorell, De Valois, and Albrecht (1984)
	1	M	Yes	167	No	Johnson, Hawken, and Shapley (2001)
Spectral bandwidth	**1**	**M**	**Yes**	**121**	**Yes**	**Thorell et al. (1984)**
Spectral peak	1	M	Yes	121	No	Thorell et al. (1984)

(*continued on next page*)

Table 1 (*continued*)

Measure	Classification method[a]	Animal[b]	Distribution reported?	*N*	Claimed segregation?	Source
Ocular dominance	1	C	Yes	223	No	Hubel and Wiesel (1962)
	1	M	Yes	272	Yes[g]	Hubel and Wiesel (1968)
	1	M	Yes	351	Yes[h]	Schiller et al. (1976b)
	1	C	Yes	272	No	Le Vay and Voigt (1988)
	2	C	Yes	89	No	Chino, Smith, Yoshida, Cheng, and Hamamoto (1994)
	2	M	Yes	239	No	Smith, Chino, Ni, Ridder, and Crawford (1997)
Multivariate statistics	**4**[i]	**M**	**Yes**	**76**	**Yes**	**Schiller, Finlay, Volman (1976e)**
	3	**C**	**Yes**	**62**	**Yes**	**Dean and Tolhurst (1983)**

The studies highlighted in bold are discussed in the text.

[a] Classification method is coded as follows: 1 = classification based solely on Hubel and Wiesel criteria, 2 = Classification based solely on F_1/F_0, 3 = classification based on Hubel and Wiesel criteria cross-validated by the F_1/F_0 ratio, 4 = Other (specified in a footnote), NA (classification method not reported in the study).

[b] Animal species was coded as follows: C = cat, M = monkey.

[c] cf. Skottun et al. (1991).

[d] F_2/F_1 for contrast reversing gratings.

[e] No quantitative data was reported to support this conclusion.

[f] Unconventional method based on moving bars.

[g] A subjective rating was used. Also, Fig 14 in Hubel and Wiesel (1968) shows no bimodality of ocular dominance (no dip in the distribution between fully monocular and fully binocular neurons).

[h] A subjective rating was used. Also, Fig. 10 in Schiller et al. (1976b) shows no bimodality of ocular dominance for the entire population.

[i] A measure of sub-field overlap was used.

Two groups have proposed that multivariate statistics might be required to distinguish between simple and complex cells (Dean & Tolhurst, 1983; Schiller et al., 1976e). This idea has not been tested rigorously, as no adequate statistical tests were provided in these studies to demonstrate a significant clustering in the distributions. For example, Schiller and colleagues (Schiller et al. (1976e)) used two independent measures for classifying simple and complex cells. One was based on a measurement of subfield segregation (already discussed above) and another was based on an optimal linear combination of several variables, which provided an optimal canonical measure, Z, obtained by linear discriminant analysis (Table 5 in Schiller et al., 1976e). When the distribution of Z is assessed over the entire population the result is not significantly bimodal (Fig. 9(c), dip-statistic $p > 0.4$). The claimed ability of this measure to classify cells into simple and complex with little errors (Table 3 in Schiller et al., 1976e) might again be a consequence of a correlation between Z and the measure of subfield segregation. Dean and Tolhurst (1983) plotted the joint distribution of two pairs of variables on the plane (their Fig. 7) for a small sample without any statistical analysis of grouping. However, the pair of statistics more suggestive of clustering included the F_1/F_0 ratio and is subject to the problems discussed here.

A possible approach to circumvent the complications introduced by rectification is to analyze the intracellular potentials of V1 neurons in vivo. As discussed above, the intracellular distributions of response modulation and mean in response to drifting gratings may help decide if two distinct classes of cells indeed exist in the cortex. The only data available do not show such a dichotomy (Carandini & Ferster, 2000), but this could be the result of the small sample in this study. Interestingly, these authors conjectured, without elaboration, that thresholding might enhance the intracellular modulation ratio to generate an extracellular bimodal distribution. Our study shows that this is indeed a possibility.

We conclude that, at present, the notion that V1 contains two discrete classes of simple and complex cells remains without convincing experimental support. A recent study of a recurrent network model of the visual cortex showed that simple and complex cells could emerge as the low- and high-gain limits of the same basic cortical circuit (Chance, Nelson, & Abbott, 1999), which is supported by preliminary experimental evidence Rivadulla, Sharma, and Sur (2001). This more uniform view of the cortical architecture stands in sharp contrast with the classical hierarchical scheme, where complex cells are built from simple cells. Our findings indicate that the possibility of a continuum of cell properties and a more uniform cortical architecture should be considered seriously. One may also conjecture that the relative variation in the number of "simple" and "complex" neurons across the V1 layers may reflect variations in the "gain" of the local feedback circuitry.

Finally, the non-linear phenomenon described here might be perceived as being particular to the F_1/F_0 statistic and unlikely to emerge in other contexts. This is not the case. For example, a second measure that suffers

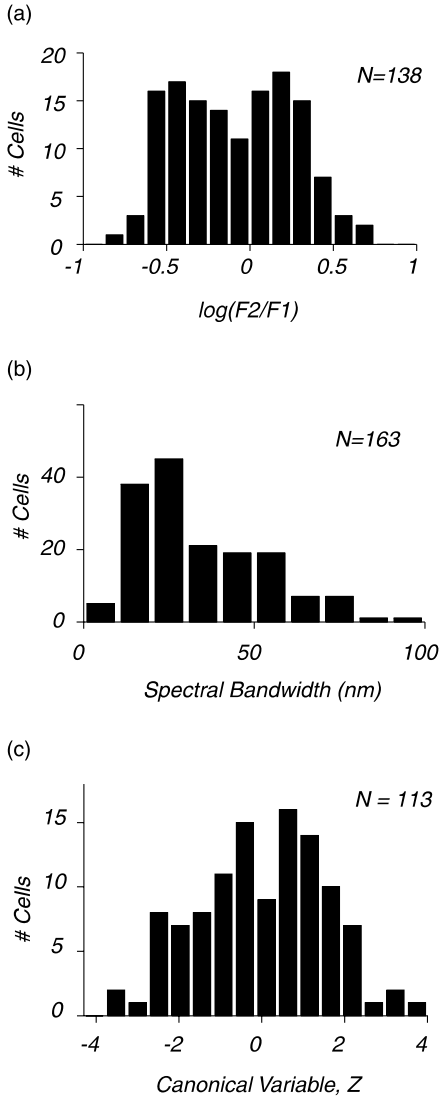

Fig. 9. (a) Distribution of F_2/F_1 in response to contrast reversing gratings in the macaque monkey (adapted from Fig. 4 in Hawken & Parker (1987)), (b) distribution of spectral bandwidths re-plotted from Fig. 5 in Thorell et al., 1984, (c) distribution of the canonical variable from Table 5 in (Schiller, Finlay, & Volman (1976e)).

from a non-linear distortion effect is the "orientation bias" or "circular variance" (Mardia, 1972) widely used to quantify the degree of orientation or direction selectivity in cortical tuning curves (Leventhal, Thompson, Liu, Zhou, & Ault, 1995; Sato, Katsuyama, Tamura, Hata, & Tsumoto, 1996; Worgotter & Eysel, 1987, among others). This measure is mathematically equivalent to the F_1/F_0 ratio, except that the independent variable is stimulus orientation (or direction) instead of time. The bimodality of circular variance recently reported in simple cells (Ringach, Shapley, & Hawken, 2001) could, in principle, have a similar explanation to the one offered here for the distribution of F_1/F_0. Thus, a general lesson from these results is that appropriate care should be given to the definition of measures and indices based on extracellular activity and in the interpretation of the resulting distributions.

Acknowledgements

We thank Bob Shapley, Michael Hawken, Matteo Carandini, Daniel Reich, Jonathan Victor, Tony Movshon, Bruce Cummings, Sheila Nirenberg and Steve Engel, and our reviewers, for helpful suggestions, comments and criticisms. The data in Fig. 4(c) have been collected in the laboratory of Robert Shapley and Michael Hawken at NYU. Supported by grants from NIH-EY-9314 (FM), NIH-EY-12816 (DLR) and NSF-IBN-9720305 (DLR).

Appendix A

A.1. Half-rectification

Given the instantaneous spike rate of the neuron, $r(t) = [a\cos(2\pi ft) - b]^+$, we would like to calculate the mean response, F_0, the first harmonic amplitude, F_1, and the ratio F_1/F_0. Without loss of generality we can assume $f = 1/2\pi$. For $-1 < b/a < 1$, when $r(t) < 0$ for some value of t we have:

$$F_0 = \frac{1}{2\pi}\int_0^{2\pi} [a\cos t - b]^+ \,\mathrm{d}t = \frac{1}{2\pi}\int_{-\theta}^{\theta} (a\cos t - b)\,\mathrm{d}t$$
$$= \frac{1}{2\pi}(2a\sin\theta - 2b\theta), \tag{A.1}$$

where θ is defined as the positive angle for which $r(t) = 0$. This occurs when $\theta = \arccos(b/a) = \arccos(\chi)$. Substituting θ in Eq. (A.1) we obtain:

$$F_0 = \frac{1}{\pi}[a\sin\theta - b\theta]$$
$$= \frac{1}{\pi}[a\sin(\arccos(b/a)) - b\ \arccos(b/a)]$$
$$= \frac{1}{\pi}\left[\sqrt{b^2 - a^2} - b\ \arccos(b/a)\right]$$
$$= \frac{a}{\pi}\left(\sqrt{1-\chi^2} - \chi\ \arccos(\chi)\right). \tag{A.2}$$

The first harmonic amplitude is given by:

$$F_1 = \frac{1}{\pi}\int_0^{2\pi} [a\cos t - b]^+ \cos t\,\mathrm{d}t$$
$$= \frac{1}{\pi}\int_{-\theta}^{\theta} \left(a\cos^2 t - b\cos t\right)\mathrm{d}t$$
$$= \frac{1}{\pi}[a\theta + a\sin(2\theta)/2 - 2b\sin\theta]$$
$$= \frac{1}{\pi}[a\theta + a\sin(\theta)\cos(\theta) - 2b\sin\theta]. \tag{A.3}$$

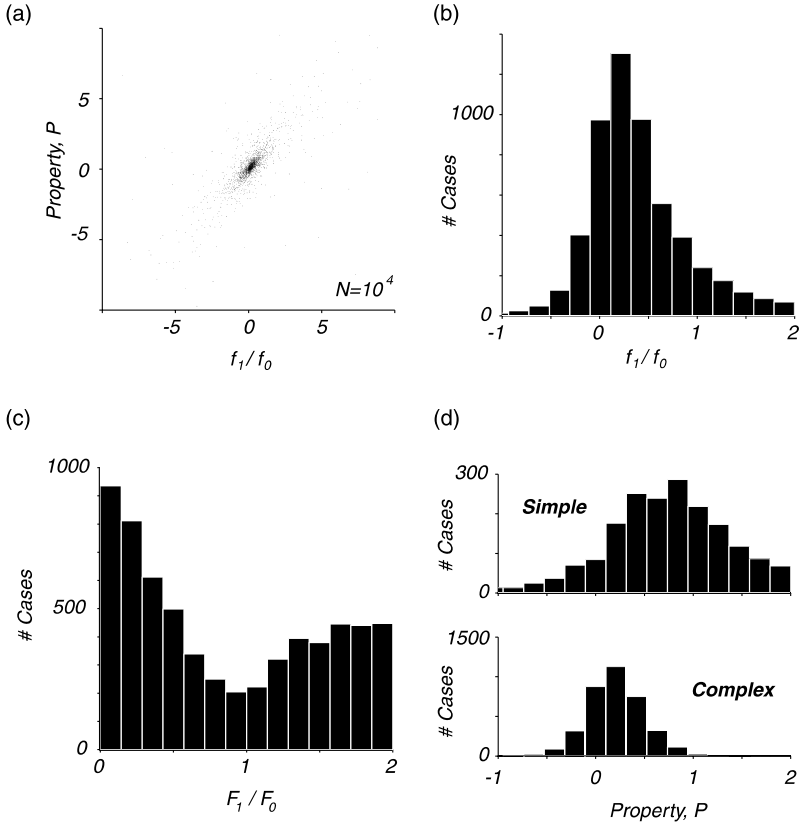

Fig. 10. Differences between "simple" and "complex" cells in other receptive field properties could be due to a correlation between the property under study and the f_1/f_0 ratio. (a) Scatter-plot of a hypothetical receptive field property P and the f_1/f_0 ratio, (b) distribution of the f_1/f_0 ratio. The distribution is unimodal and, due to the correlation with P, very similar to the distribution of P itself, (c) the distribution of F_1/F_0 is bimodal and can be used to define "simple" and "complex" cells, (d) separate distributions of P for simple and complex cells as defined using the F_1/F_0 ratio. The means of the distributions are significantly different.

By substituting $\theta = a\cos(b/a)$ we get

$$\begin{aligned} F_1 &= \frac{1}{\pi}\left[a\arccos(b/a) + a\sqrt{1-(b/a)^2}(b/a) \right. \\ &\quad \left. - 2b\sqrt{1-(b/a)^2}\right] \\ &= \frac{1}{\pi}\left[a\arccos(b/a) - b\sqrt{1-(b/a)^2}\right] \\ &= \frac{a}{\pi}\left[\arccos(\chi) - \chi\sqrt{1-\chi^2}\right]. \end{aligned} \tag{A.4}$$

Thus, the F_1/F_0 ratio, when $-1 \leqslant \chi \leqslant 1$, is given by

$$F_1/F_0 = \frac{-\chi\sqrt{1-\chi^2} + \arccos(\chi)}{\sqrt{1-\chi^2} - \chi\ \arccos(\chi)}. \tag{A.5}$$

When $\chi < -1$ the modulation is never rectified ($r(t) > 0$ for all t) and we have that $F_0 = -b$ and $F_1 = a$. Thus, in this case,

$$F_1/F_0 = -1/\chi. \tag{A.6}$$

A.2. Half-squaring

Because half-squaring is a commonly used non-linearity in modeling (Heeger, 1992) we present a closed-form solution for this case as well. Here, the instantaneous spike rate is given by

$$r(t) = \left([a\cos(t) - b]^+\right)^2.$$

Again, F_1/F_0 is only defined for cases in which $r(t) > 0$. We employ the same notation as above and denote $\chi = b/a$ and $\theta = \arccos(\chi)$. For $-1 < \chi < 1$, $r(t) > 0$ if $-\theta < t < \theta$, and for $\chi < -1$, $r(t) > 0$ if $-\pi < t < \pi$. The mean spike rate in the first case is given by:

$$\begin{aligned} F_0 &= \frac{1}{2\pi}\int_{-\theta}^{+\theta} (-b + a\cos(t))^2\,\mathrm{d}t \\ &= \frac{a^2}{\pi}\int_0^{\theta}\left(\left(\frac{b}{a}\right)^2 - 2\frac{b}{a}\cos(t) + \cos^2(t)\right)\mathrm{d}t \\ &= \frac{a^2}{\pi}\left[\chi^2\theta - 2\chi\sin(\theta) + \left(\frac{\theta}{2} + \frac{1}{2}\sin(\theta)\cos(\theta)\right)\right] \\ &= \frac{a^2}{\pi}\left[\theta\left(\chi^2 + \frac{1}{2}\right) - \sin(\theta)\left(2\chi - \frac{1}{2}\cos(\theta)\right)\right] \\ &= \frac{a^2}{\pi}\left[\frac{1}{2}\left(2\chi^2+1\right)\arccos(\chi) - \frac{3}{2}\chi\sqrt{1-\chi^2}\right]. \end{aligned} \tag{A.7}$$

and the first harmonic amplitude is given by

$$
\begin{aligned}
F_1 &= \frac{1}{\pi}\int_{-\theta}^{+\theta} \cos(t)(-b + a\cos(t))^2\,\mathrm{d}t \\
&= \frac{2a^2}{\pi}\int_0^{\theta}\left(\left(\frac{b}{a}\right)^2\cos(t) - 2\frac{b}{a}\cos^2(t) + \cos^3(t)\right)\mathrm{d}t \\
&= \frac{2a^2}{\pi}\left[\chi^2\sin(\theta) - 2\chi\left(\frac{\theta}{2} + \frac{1}{2}\sin(\theta)\cos(\theta)\right)\right. \\
&\quad \left. + \left(\sin(\theta) - \frac{1}{3}\sin^3(\theta)\right)\right] \\
&= \frac{2a^2}{\pi}\left[\chi^2\sin(\theta) - 2\chi\frac{\theta}{2} - 2\chi\frac{1}{2}\sin(\theta)\cos(\theta)\right. \\
&\quad \left. + \frac{\sin(\theta)}{3}\left(2 + \cos^2(\theta)\right)\right] \\
&= \frac{2a^2}{\pi}\left[-\chi\arccos(\chi) + \sqrt{1-\chi^2}\left(\chi^2 - \chi^2 + \frac{2}{3} + \frac{1}{3}\chi^2\right)\right] \\
&= \frac{a^2}{\pi}\left[-2\chi\arccos(\chi) + \frac{2}{3}\left(2+\chi^2\right)\sqrt{1-\chi^2}\right], \qquad \text{(A.8)}
\end{aligned}
$$

which yields,

$$
F_1/F_0 = \frac{4}{3}\frac{(2+\chi^2)\sqrt{1-\chi^2} - 3\chi\arccos(\chi)}{-3\chi\sqrt{1-\chi^2} + (2\chi^2+1)\arccos(\chi).} \qquad \text{(A.9)}
$$

When $-\infty < \chi < -1$, the mean spike rate is given by:

$$
\begin{aligned}
F_0 &= \frac{1}{2\pi}\int_{-\pi}^{\pi}(-b + a\cos(t))^2\,\mathrm{d}t \\
&= \frac{a^2}{\pi}\int_0^{\pi}\left(\left(\frac{b}{a}\right)^2 - 2\frac{b}{a}\cos(t) + \cos^2(t)\right)\mathrm{d}t \\
&= \frac{a^2}{\pi}\left[\pi\chi^2 - 0 + \frac{\pi}{2}\right] = \frac{a^2}{2}\left(2\chi^2+1\right) \qquad \text{(A.10)}
\end{aligned}
$$

and the first-harmonic response is,

$$
\begin{aligned}
F_1 &= \frac{1}{\pi}\int_{-\pi}^{\pi}\cos(t)(-b + a\cos(t))^2\,\mathrm{d}t \\
&= \frac{2a^2}{\pi}\int_0^{\pi}\left(\left(\frac{b}{a}\right)^2\cos(t) - 2\frac{b}{a}\cos^2(t) + \cos^3(t)\right)\mathrm{d}t \\
&= \frac{2a^2}{\pi}\left[0 - 2\chi\frac{\pi}{2} + 0\right] = \frac{a^2}{2}(-4\chi), \qquad \text{(A.11)}
\end{aligned}
$$

so, in this case, their ratio is given by

$$
F_1/F_0 = \frac{-4\chi}{2\chi^2+1}. \qquad \text{(A.12)}
$$

A.3. General solution for a power non-linearity

It is possible to provide general solutions for the case where the non-linearity is power-law. We provide these expressions here for completeness, without a full derivation. We denote by $g(p,\chi)$ the first-harmonic to DC ratio at χ for a power-law non-linearity with exponent p. First, if p is a non-negative real the following recursive relationship applies:

$$
g(p,\chi) = \frac{2p}{p+1}\frac{2 - \chi g(p-1,\chi)}{g(p-1,\chi) - 2\chi} \quad \text{for } p \in \mathbb{R}^+. \qquad \text{(A.13a)}
$$

The initial condition is easy to obtain for $p = 0$

$$
g(0,\chi) = \begin{cases} 0 & \text{if } \chi < -1 \\ 2\sqrt{1-\chi^2}/\arccos(\chi) & \text{if } -1 < \chi < 1. \end{cases} \qquad \text{(A.13b)}
$$

Thus these equations allow one to easily calculate $g(p,\chi)$ recursively for any power-law with an integer exponent $(p = 1, 2, 3, \ldots)$. Note that an exponent of $p = 0$ corresponds to a step non-linearity.

A more complex closed form expression applies for the general case of a real exponent. In this case we obtain, with help from the Mathematica symbolic package (Wolfram Research), the following expressions. For $\chi < -1$:

$$
g(p,\chi) = 2\frac{(A-B)(-\chi-1)^p + (C-D)(1-\chi)^p}{B(-\chi-1)^p + C(1-\chi)^p}, \qquad \text{(A.14)}
$$

where

$$
\begin{aligned}
A &= {}_2F_1(3/2, -p; 2; 2/(\chi+1)) \\
B &= {}_2F_1(1/2, -p; 1; 2/(\chi+1)) \\
C &= {}_2F_1(1/2, -p; 1; -2/(\chi-1)) \\
D &= {}_2F_1(3/2, -p; 2; -2/(\chi-1)) \qquad \text{(A.15)}
\end{aligned}
$$

and ${}_2F_1(a,b;c;d)$ is the Gauss hypergeometric function. For $-1 < \chi < 1$ the result is:

$$
g(p,\chi) = 2\left\{\chi - \frac{(\chi-1)(p+1)\,{}_2\bar{F}_1(1/2, p+2; p+5/2; (\chi-1)/(\chi+1))}{{}_2\bar{F}_1(1/2, p+1; p+3/2; (\chi-1)/(\chi+1))}\right\}, \qquad \text{(A.16)}
$$

where ${}_2\bar{F}_1(a,b;c;d) = {}_2F_1(a,b;c;d)/\Gamma(c)$ is the regularized hypergeometric function.

A.4. Relationship between the intracellular and extracellular modulation ratios

In the main text, we have shown that, for a large class of threshold operators, including half-rectification, the F_1/F_0 extracellular ratio is a function of a single dimensionless parameter χ. Let us denote the intracellular modulation amplitude f_1, and the mean by f_0. With the notation already introduced, and by rescaling the potential $V = v'(V_{\mathrm{th}} - V_{\mathrm{rest}})$ we write:

$$
\begin{aligned}
f_0 &= V_{\mathrm{mean}} - V_{\mathrm{rest}} = (V_{\mathrm{th}} - V_{\mathrm{rest}}) - (V_{\mathrm{th}} - V_{\mathrm{mean}}) \\
&= (V_{\mathrm{th}} - V_{\mathrm{rest}})\left(v'_{\mathrm{th}} - b'\right) \\
f_1 &= a = (V_{\mathrm{th}} - V_{\mathrm{rest}})a' \qquad \text{(A.17a)}
\end{aligned}
$$

or

$$
\begin{aligned}
f'_0 &= \left(1 - b'\right) \\
f'_1 &= a' \qquad \text{(A.17b)}
\end{aligned}
$$

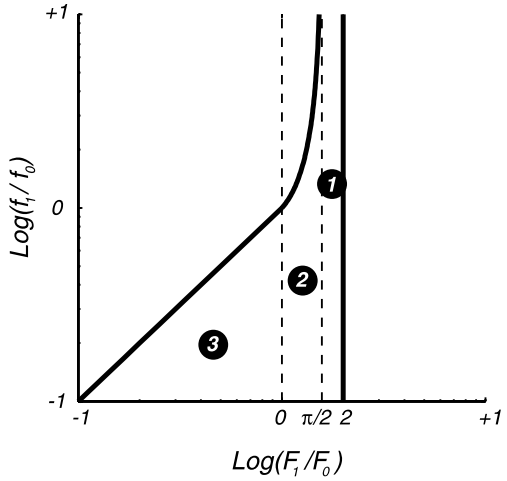

Fig. 11. Theoretical boundaries in the $(F_1/F_0, f_1/f_0)$ plane. The numbers in circles indicate the regions defined by each of the different cases considered, (1) $0 < \chi < 1$, (2) $-1 < \chi < 0$ and (3) $-\infty < \chi < -1$.

so we can write for the intracellular modulation ratio

$$\frac{f_1}{f_0} = \frac{f_1'}{f_0'} = \frac{a'}{1-b'} = \frac{a'}{1-a'\chi}, \tag{A.18}$$

because $\chi' = a'/b' = a/b = \chi$. Notice that in addition to the ratio of modulation and mean, the intracellular modulation ratio depends also on the magnitude of the modulation. For a fixed χ, the intracellular modulation ratio is a function of the modulation amplitude:

$$\frac{f_1}{f_0} \equiv h_\chi(a') = \frac{a'}{1-\chi a'}. \tag{A.19}$$

On the other hand, the extracellular modulation ratio, for a given χ, is constant. Therefore, the intracellular and extracellular modulation ratios are not related by one-to-one mapping.

Eq. (A.19) can be used to derive theoretical bounds within which points in the $(F_1/F_0, f_1/f_0)$ plane should fall. We have already established that $-\infty < \chi < 1$. We consider the following cases:

Case 1. $0 < \chi < 1$. Then, $f_1/f_0 \to \infty$ as $a' \to 1/\chi$ from the left. Thus, all points within the region $g(0) = \pi/2 < F_1/F_0 < 2 = g(1)$ and $f_1/f_0 > 0$ are admissible.

Case 2. $-1 < \chi < 0$. In this case, all points within the region $g(-1) = 1 < F_1/F_0 < \pi/2 = g(0)$ and $0 < f_1/f_0 < -1/\chi$ are admissible.

Case 3. $-\infty < \chi < -1$. In this case, all points within the region $g(-\infty) = 0 < F_1/F_0 < 1 = g(-1)$ and $0 < f_1/f_0 < -1/\chi$ are admissible. In this interval we have that $F_1/F_0 = -1/\chi$ and the upper bound of f_1/f_0 at that location is also given by $f_1/f_0 < -1/\chi$. Therefore, the top boundary in the $(F_1/F_0, f_1/f_0)$ plane when $-\infty < \chi < -1$ is the unity line.

The resulting theoretical boundaries produced by these considerations are summarized in Fig. 11.

References

Albrecht, D. G., Valois, R. L., & Thorell, L. G. (1980). Visual cortical neurons: Are bars or gratings the optimal stimuli? *Science, 207*, 88–90.

Albrecht, D. G., & Geisler, W. S. (1991). Motion selectivity and the contrast-response function of simple cells in the visual cortex. *Visual Neuroscience, 7*(6), 531–546.

Anzai, A., Ohzawa, I., & Freeman, R. D. (1999). Neural mechanisms for processing binocular information I. Simple cells. *Journal of Neurophysiology, 82*, 891–908.

Bonds, A. B. (1991). Temporal dynamics of contrast gain in single cells of the cat striate cortex. *Visual Neuroscience, 6*, 239–255.

Carandini, M., Mechler, F., Leonard, C. S., & Movshon, J. A. (1996). Spike train encoding by regular-spiking cells of the visual cortex. *Journal of Neurophysiology, 76*, 3425–3441.

Carandini, M., & Ferster, D. (2000). Membrane potential and firing rate in cat primary visual cortex. *Journal of Neuroscience, 20*, 470–484.

Casanova, C., Nordmann, J. P., Ohzawa, I., & Freeman, R. D. (1992). Direction selectivity of cells in the cat's striate cortex: differences between bar and grating stimuli. *Visual Neuroscience, 9*, 505–513.

Cattaneo, A., Maffei, L., & Morrone, C. (1981). Patterns in the discharge of simple and complex visual cortical cells. *Proceedings of the Royal Society of London Series-B Biological Sciences, 212*, 279–297.

Chance, F. S., Nelson, S. B., & Abbott, L. F. (1999). Complex cells as cortically amplified simple cells. *Nature Neuroscience, 2*, 277–282.

Chino, Y. M., Smith, E. L., III, Yoshida, K., Cheng, H., & Hamamoto, J. (1994). Binocular interactions in striate cortical neurons of cats reared with discordant visual inputs. *Journal of Neuroscience, 14*, 5050–5067.

Cumming, B. G., Thomas, O. M., Parker, A. J., & Hawken, M. J. (1999). Classification of simple and complex cells in V1 of the awake monkey. *Society for Neuroscience Abstracts, 25*, 1548.

De Busk, B. C., De Bruyn, E. J., Snider, R. K, Kabara, J. F., & Bonds, A. B. (1997). Stimulus-dependent modulation of spike burst length in cat striate cortical cells. *Journal of Neurophysiology, 78*(1), 199–213.

De Valois, R. L., Albrecht, D. G., & Thorell, L. G. (1982). Spatial frequency selectivity of cells in macaque visual cortex. *Vision Research, 22*, 545–559.

Dean, A. F. (1981). The relationship between response amplitude and contrast for cat striate cortical neurones. *Journal of Physiology-London, 318*, 413–427.

Dean, A. F., & Tolhurst, D. J. (1983). On the distinctness of simple and complex cells in the visual cortex of the cat. *Journal of Physiology-London, 344*, 305–325.

De Angelis, G. C., Freeman, R. D., & Ohzawa, I. (1994). Length and width tuning of neurons in the cat's primary visual cortex. *Journal of Neurophysiology, 71*, 347–374.

Gilbert, C. D. (1977). Laminar differences in receptive field properties of cells in cat primary visual cortex. *Journal of Physiology-London, 268*, 391–421.

Hammond, P., & Munden, I. M. (1990). Areal influences on complex cells in cat striate cortex: stimulus-specificity of width and length summation. *Experimental Brain Research, 80*, 135–147.

Hartigan, J. A., & Hartigan, P. M. (1985). The dip test of unimodality. *Annals of Statistics, 13*, 70–84.

Hawken, M. J., & Parker, A. J. (1987). Spatial properties of neurons in the monkey striate cortex. *Proceedings of the Royal Society of London Series-B Biological Sciences, 231*, 251–288.

Hawken, M. J., Parker, A. J., & Lund, J. S. (1988). Laminar organization and contrast sensitivity of direction-selective cells in the striate cortex of the Old World monkey. *Journal of Neuroscience, 8*, 3541–3548.

Hawken, M. J., Shapley, R. M., & Grosof, D. H. (1996). Temporal-frequency selectivity in monkey visual cortex. *Visual Neuroscience, 13*, 477–492.

Heggelund, P., & Albus, K. (1978). Response variability and orientation discrimination of single cells in striate cortex of cat. *Experimental Brain Research, 32*, 197–211.

Heeger, D. J. (1992). Normalization of cell responses in cat striate cortex. *Visual Neuroscience, 9*(2), 181–197.

Hubel, D. H., & Wiesel, T. N. (1962). Receptive fields, binocular interaction and functional architecture in the cat's visual cortex. *Journal of Physiology-London, 160*, 106–154.

Hubel, D. H., & Wiesel, T. N. (1968). Receptive fields and functional architecture of monkey striate cortex. *Journal of Physiology-London, 195*, 215–243.

Jagadeesh, B., Wheat, H. S., Kontsevich, L. L., Tyler, C. W., & Ferster, D. (1997). Direction selectivity of synaptic potentials in simple cells of the cat visual cortex. *Journal of Neurophysiology, 78*, 2772–2789.

Johnson, E. N., Hawken, M. J., & Shapley, R. (2001). The spatial transformation of color in the primary visual cortex of the macaque monkey. *Nature Neuroscience, 4*, 409–416.

Lampl, I., Anderson, J. S., Gillespie, D. C., & Ferster, D. (2001). Prediction of orientation selectivity from receptive field architecture in simple cells of cat visual cortex. *Neuron, 30*, 263–274.

Le Vay, S., & Voigt, T. (1988). Ocular dominance and disparity coding in cat visual cortex. *Visual Neuroscience, 1*, 395–414.

Leventhal, A. G., Thompson, K. G., Liu, D., Zhou, Y., & Ault, S. J. (1995). Concomitant sensitivity to orientation, direction, and color of cells in layers 2, 3, and 4 of monkey striate cortex. *Journal of Neuroscience, 15*, 1808–1818.

Lennie, P., Krauskopf, J., & Sclar, G. (1990). Chromatic mechanisms in striate cortex of macaque. *Journal of Neuroscience, 10*, 649–669.

Maffei, L., & Fiorentini, A. (1973). The visual cortex as a spatial frequency analyser. *Vision Research, 13*(7), 1255–1267.

Mardia, K. V. (1972). *Statistics of directional data*. New York: Academic Press.

Maunsell, J. H., & Gibson, J. R. (1992). Visual response latencies in striate cortex of the macaque monkey. *Journal of Neurophysiology, 68*, 1332–1344.

Movshon, J. A., Thompson, I. D., & Tolhurst, D. J. (1978a). Receptive field organization of complex cells in the cat's striate cortex. *Journal of Physiology-London, 283*, 79–99.

Movshon, J. A., Thompson, I. D., & Tolhurst, D. J. (1978b). Spatial and temporal contrast sensitivity of neurones in areas 17 and 18 of the cat's visual cortex. *Journal of Physiology-London, 283*, 101–120.

Ohzawa, I., Sclar, G., & Freeman, R. D. (1985). Contrast gain control in the cat's visual system. *Journal of Neurophysiology, 54*, 651–667.

Ohzawa, I., De Angelis, G. C., & Freeman, R. D. (1996). Encoding of binocular disparity by simple cells in the cat's visual cortex. *Journal of Neurophysiology, 75*, 1779–1805.

Ohzawa, I., DeAngelis, G. C., & Freeman, R. D. (1997). Encoding of binocular disparity by complex cells in the cat's visual cortex. *Journal of Neurophysiology, 77*, 2879–2909.

Papoulis, A. (1984). *Probability, random variables, and stochastic processes* (2nd ed.). New York: McGraw-Hill.

Pettigrew, J. D., Nikara, T., & Bishop, P. O. (1968). Responses to moving slits by single units in cat striate cortex. *Experimental Brain Research, 6*, 373–390.

Ringach, D. L., Shapley, R., & Hawken, M. J. (2001). Bimodal distribution of orienatation selectivity in simple cells of Macaque V1. *Investigative Ophthalmology and Visual Science, 42*, S726.

Rivadulla, C., Sharma, J., & Sur, M. (2001). Specific roles of NMDA and AMPA receptors in direction-selective and spatial phase-selective responses in visual cortex. *Journal of Neuroscience, 21*(5), 1710–1719.

Sato, H., Katsuyama, N., Tamura, H., Hata, Y., & Tsumoto, T. (1996). Mechanisms underlying orientation selectivity of neurons in the primary visual cortex of the macaque. *Journal of Physiology-London, 494*(Part 3), 757–771.

Sceniak, M. P., Ringach, D. L., Hawken, M. J., & Shapley, R. (1999). Contrast's effect on spatial summation by macaque V1 neurons. *Nature Neuroscience, 2*, 733–739.

Schiller, P. H., Finlay, B. L., & Volman, S. F. (1976a). Quantitative studies of single-cell properties in monkey striate cortex. III. Spatial frequency. *Journal of Neurophysiology, 39*, 1334–1351.

Schiller, P. H., Finlay, B. L., & Volman, S. F. (1976b). Quantitative studies of single-cell properties in monkey striate cortex. II. Orientation specificity and ocular dominance. *Journal of Neurophysiology, 39*, 1320–1333.

Schiller, P. H., Finlay, B. L., & Volman, S. F. (1976c). Quantitative studies of single-cell properties in monkey striate cortex. I. Spatiotemporal organization of receptive fields. *Journal of Neurophysiology, 39*, 1288–1319.

Schiller, P. H., Finlay, B. L., & Volman, S. F. (1976d). Short-term response variability of monkey striate neurons. *Brain Research, 105*, 347–349.

Schiller, P. H., Finlay, B. L., & Volman, S. F. (1976e). Quantitative studies of single-cell properties in monkey striate cortex. V. Multivariate statistical analyses and models. *Journal of Neurophysiology, 39*, 1362–1374.

Skottun, B. C., Bradley, A., Sclar, G., Ohzawa, I., & Freeman, R. D. (1987). The effects of contrast on visual orientation and spatial frequency discrimination: a comparison of single cells and behavior. *Journal of Neurophysiology, 57*, 773–786.

Skottun, B. C., De Valois, R. L., Grosof, D. H., Movshon, J. A., Albrecht, D. G., & Bonds, A. B. (1991). Classifying simple and complex cells on the basis of response modulation. *Vision Research, 31*, 1079–1086.

Smith, E. L., III, Chino, Y. M., Ni, J., Ridder, W. H., III, & Crawford, M. L. (1997). Binocular spatial phase tuning characteristics of neurons in the macaque striate cortex. *Journal of Neurophysiology, 78*, 351–365.

Swindale, N. V., & Cynader, M. S. (1989). Vernier acuities of neurons in area 17 of cat visual cortex: their relation to stimulus length and velocity orientation selectivity and receptive-field structure. *Visual Neuroscience, 2*, 165–176.

Tao, L., Shelley, M. J., Shapley, R. M., & McLaughlin, D. W. (2001). *How complex cells are made in a simple cell network*. San Diego, California: Society for Neuroscience Annual Meeting.

Thorell, L. G., De Valois, R. L., & Albrecht, D. G. (1984). Spatial mapping of monkey V1 cells with pure color and luminance stimuli. *Vision Research, 24*, 751–769.

Tomko, G. J., & Crapper, D. R. (1974). Neuronal variability: non-stationary responses to identical visual stimuli. *Brain Research, 79*, 405–418.

Wörgötter, F., & Eysel, U. T. (1987). Quantitative determination of orientational and directional components in the response of visual cortical cells to moving stimuli. *Biological Cybernetics, 57*, 349–355.